

Multichannel Adjustable Single-Photon Router Based on Large Detuning

Jia-Nan Wu,¹ Junhua Dong¹,^{*} Yafang Xu,² Bingsuo Zou,³ and Yongyou Zhang¹^{*}

¹*Beijing Key Laboratory of Nanophotonics & Ultrafine Optoelectronic Systems, School of Physics, Beijing Institute of Technology, Beijing 100081, China*

²*College of Physics Science and Technology, Yangzhou University, Yangzhou 225002, China*

³*MOE & Guangxi Key Laboratory of Processing for Non-ferrous Metals and Featured Materials, School of Physical science and Technology, Guangxi University, Nanning 530004, China*



(Received 21 December 2021; revised 4 June 2022; accepted 16 September 2022; published 2 November 2022)

Quantum router as a key device in quantum information processing always attracts researchers' attention. This work suggests a single-photon (SP) router based on one bus-waveguide side coupled to numerous Jaynes-Cummings emitters (JCEs). Each JCE connects with a semi-infinite branch waveguide as an output channel. Different from the commonly used scheme that the JCEs are set in the tuning regime, we here let them work in the large-detuning regime. This change brings about the following amazing benefits for the SP router. Firstly, the number of channels can reach more than a thousand. Secondly, the router is adjustable, that is, the SP can be routed into any output channel on demand. Thirdly, the router has a remarkable monochromaticity. Fourthly, such a SP router can also depress the influence of cavity losses and interferential levels in atoms. Finally, the routing probability can reach approximately 100% for each channel by adding a mirror and a phase shifter to the end of the bus waveguide. This work takes the Rydberg atoms ^{87}Rb whose levels can be adjusted by an external electrostatic field as an example to demonstrate the feasibility of the router, which can be applied to quantum informatics.

DOI: 10.1103/PhysRevApplied.18.054007

I. INTRODUCTION

One-dimensional waveguide-QED systems [1] in recent decades have deeply attracted researchers due to their simple structures and extensive applications in quantum informatics. The waveguides are often coupled to quantum emitters like quantum dots [2,3], two-level systems [4], such as two-level atoms [5], and side optical cavities [6]. Sometimes side optical cavities contain two-level atoms to form the so-called Jaynes-Cummings emitters (JCEs) [7] or contain Kerr medium [8]. It is these waveguide-based architectures that rouse the development in the waveguide-QED field. Researchers have discovered many significant phenomena, such as electromagnetically induced transparency [9,10], Fano resonance [11,12], polarization effect [13], slow light behavior [9], and multiphoton transmission [14,15], which are used to design optical switches [16,17], quantum circuits [18], superconducting single-photon (SP) detectors [19], SP transistors [20], photon memories [21], band filters [22], and many other potential devices [23,24].

Quantum routers, routing the incident quantum bits to different output ports with phase coherence, are a key type of building block in quantum information processing. The control signals can be either quantum or classical,

corresponding to the fully quantum routers [25,26] or classically controlled ones [27–29], respectively. The quantum routers have been implemented on the platforms of superconducting circuits [26,30,31] and waveguide-QED systems [32]. Using waveguide-QED systems, researchers have suggested a number of schemes for the SP routing [27,28,33–45], but most of which have too few channels [27,28,38,42,45–47]. Note that the channels here represent the waveguides for outputting signals, rather than the commonly used notion in information processing, i.e., a frequency range within the work band of a device. By controlling the transition energies of the two-level systems and their coupling strengths with the waveguides, researchers could also achieve the SP router with multiple channels [36]. In view of application, these quantum routers, generally speaking, need improvement in part or all of the following aspects. Firstly, improving the number of channels to satisfy the need of information transport. Secondly, improving the adjustability of the routers to allow users to change the output channel for a SP in a settled architecture. Thirdly, the routing channel in most of the proposed quantum routers is commonly not monochromatic and therefore, can accept many plane-wave components [27,46], which makes it difficult to classify a great deal of information. This third point leads to the fourth one, that is, if the spectra of output channels have very narrow peaks, the quantum routers should depend less on the system losses.

*yyzhang@bit.edu.cn

To overcome these disadvantages, this work puts forward an alternative scheme to realize the SP quantum router that is not only adjustable but also can hold plenty of output channels. The background physics is to let the JCEs work in the large-detuning regime [49], different from those previously proposed routers where the JCEs work in the tuning regime. Our model, schematically plotted in Fig. 1(a), consists of a bus waveguide and N semi-infinite branch ones, similar to the structure used in Ref. [50]. The bus and branch waveguides are taken as the input channel and output ones, respectively. Each branch waveguide is bridged to the bus one by a JCE. Note that there is only one terminal in the semi-infinite branch waveguide

for the SP output, while there are two in the infinite waveguide. Accordingly, the branch waveguides are taken to be semi-infinite here to benefit the routing probability. We focus on the microwave band, as an example, to demonstrate the feasibility of the model in this work, that is, around the angular frequency of $\omega_0 = 2\pi \times 10^{10}$ Hz with the corresponding wavelength $\lambda_0 = 3$ cm and wave vector $k_0 \equiv 2\pi/\lambda_0$. This scheme is also suitable for other wavebands, as long as the model parameters are chosen for those. In the microwave band, every JCE is assumed to contain one microwave cavity and one embedded Rydberg atom ⁸⁷Rb.

Such a model in Fig. 1(a) can serve as a multichannel adjustable SP router and has the merits as follows: (i) the number of channels can reach more than a thousand; (ii) the SP can be routed into any output channel as required and therefore, the router is adjustable; (iii) the router not only has a remarkable monochromaticity but also (iv) can depress the influence of cavity losses and interferential levels in atoms. To discuss such a router, this work is organized as follows. In Sec. II, we firstly introduce the Hamiltonian and related parameters in the model and then derive the amplitudes of the transmission (t_n), reflection (r_n), and scattering (χ_n), denoted in Fig. 1(a). Section III includes two cases, according to whether the two-level atoms are considered or not. Based on them, why the large-detuning mechanism of the JCEs can lead to such a multichannel adjustable SP router is shown. In Sec. IV, the loss effects of cavities and two-level atoms and the influence of interferential levels in atoms are discussed. What is more, an updated scheme that can lead to the routing probability of up to approximately 100% is suggested. Since researchers have realized waveguide-QED [51] and cavity-atom [52,53] systems in experiments, including quantum routing [26,30,32], the proposed quantum router should be practical. Finally, a brief conclusion is summarized in Sec. V.

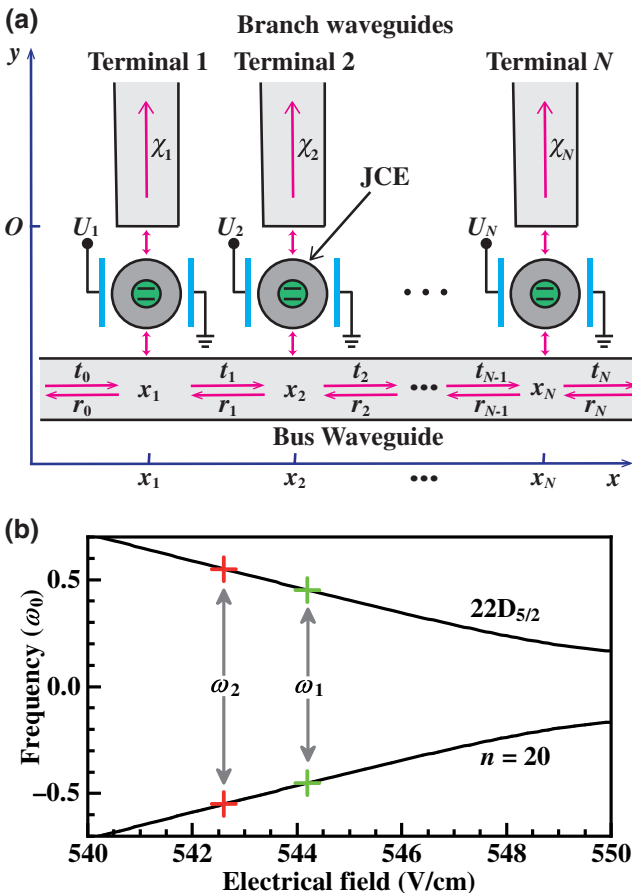


FIG. 1. (a) Schematic diagram of the bus and branch waveguides, connected by N JCEs. The n th JCE is placed at x_n . t_n , r_n , and χ_n denote the amplitudes of the transmission, reflection, and scattering in the system, respectively. There is a Rydberg atom of ⁸⁷Rb in each JCE and the transition energy between the concerned two Rydberg levels can be tuned by an external electrostatic field, as shown in (b). We focus on the transition frequency range of $[\omega_1, \omega_2] = [0.9\omega_0, 1.1\omega_0]$ with $\omega_0 = 2\pi \times 10^{10}$ Hz, where ω_1 and ω_2 correspond to the electrostatic fields of 544.2 V/cm and 542.6 V/cm, respectively. Details are in Ref. [48].

II. HAMILTONIAN AND FORMULAS

The Hamiltonian of the whole system in Fig. 1(a) can be separated into

$$H = H_{\text{bus}} + H_{\text{JCE}} + H_{\text{branch}} + H_{\text{JCE-bus}} + H_{\text{JCE-branch}}, \quad (1)$$

where H_{bus} , H_{JCE} , H_{branch} , $H_{\text{JCE-bus}}$, and $H_{\text{JCE-branch}}$, respectively, describe the bus waveguide, all JCEs, all branch waveguides, interactions between the bus waveguide and each JCE, and interactions between each JCE and corresponding branch waveguide. For convenience, the Plank constant is set to $\hbar = 1$ throughout the work. The x axis is along the horizontal direction with the n th JCE locating at x_n and the y axis is along the vertical direction with the bottom of all branch waveguides at $y = 0$, see Fig. 1(a).

The distances between any adjacent JCEs are the same, denoted as d .

In the real space, the H_{bus} reads [1]

$$H_{\text{bus}} = \int_{-\infty}^{\infty} dx \hat{R}^\dagger(x) (\omega_0 - v_g k_0 - i v_g \partial_x) \hat{R}(x) + \int_{-\infty}^{\infty} dx \hat{L}^\dagger(x) (\omega_0 - v_g k_0 + i v_g \partial_x) \hat{L}(x), \quad (2)$$

where $\hat{R}^\dagger(x)$ and $\hat{R}(x)$ [$\hat{L}^\dagger(x)$ and $\hat{L}(x)$] represent the creation and annihilation field operators for the rightward-moving (leftward-moving) photons at coordinate x in the bus waveguide. The dispersion of the bus waveguide is linearized as $\varepsilon = \omega_0 \pm v_g(k - k_0)$ at the frequency ω_0 with the corresponding wave vector k_0 and group velocity v_g . Such a linearization is reasonable in a narrow frequency range, which has been widely used for studying the transport of photons in a quantum waveguide as the nonlinear effect of the dispersions can be neglected [1,54]. In this work, the range is assumed to be $[\omega_1, \omega_2] = [0.9\omega_0, 1.1\omega_0]$.

The branch waveguides are described by the Hamiltonian H_{branch} , namely,

$$H_{\text{branch}} = \sum_{n=1}^N \int_0^{\infty} dy \hat{U}_n^\dagger(y) (\omega_0 - v_g k_0 - i v_g \partial_y) \hat{U}_n(y). \quad (3)$$

$\hat{U}_n^\dagger(y)$ and $\hat{U}_n(y)$ are the creation and annihilation operators of the upward-moving photons in the n th branch waveguide, respectively. There is no downward-moving photons in any branch waveguide. Without loss of generality, the dispersions of all branch waveguides are taken to be the same as that of the bus one.

Under an external electrostatic field, H_{JCE} has the form [17,48],

$$H_{\text{JCE}} = \sum_{n=1}^N [\tilde{\omega}_n^c \hat{c}_n^\dagger \hat{c}_n + \tilde{\omega}_n^a \hat{\sigma}_n^+ \hat{\sigma}_n^- + \Omega (\hat{c}_n^\dagger \hat{\sigma}_n^- + \hat{c}_n \hat{\sigma}_n^+)], \quad (4)$$

where $\tilde{\omega}_n^c = \omega_n^c - i\gamma_n^c$ with the eigenfrequency ω_n^c and loss γ_n^c of the n th cavity, and $\tilde{\omega}_n^a = \omega_n^a - i\gamma_n^a$ with the transition energy ω_n^a and loss γ_n^a for the ^{87}Rb in the n th cavity. The lowering (raising) operator of the ^{87}Rb is denoted as $\hat{\sigma}_n^-$ ($\hat{\sigma}_n^+$) and the annihilation (creation) one of the photon is denoted as \hat{c}_n (\hat{c}_n^\dagger). Ω measures the Rabi coupling strength between the atom and cavity in each JCE. The hybrid modes in each JCE can be found from the eigenequation,

$$\begin{pmatrix} \tilde{\omega}_n^c & \Omega \\ \Omega & \tilde{\omega}_n^a \end{pmatrix} \begin{pmatrix} z_c^\pm \\ z_a^\pm \end{pmatrix} = \varepsilon_n^\pm \begin{pmatrix} z_c^\pm \\ z_a^\pm \end{pmatrix}, \quad (5)$$

where

$$\varepsilon_n^\pm = \frac{1}{2} \left(\tilde{\omega}_n^a + \tilde{\omega}_n^c \pm \sqrt{(\tilde{\omega}_n^a - \tilde{\omega}_n^c)^2 + 4\Omega^2} \right), \quad (6)$$

$$z_c^\pm = \Omega / \sqrt{(\varepsilon_n^\pm - \tilde{\omega}_n^c)^2 + \Omega^2}, \quad (7)$$

$$z_a^\pm = (\varepsilon_n^\pm - \tilde{\omega}_n^a) / \sqrt{(\varepsilon_n^\pm - \tilde{\omega}_n^a)^2 + \Omega^2}. \quad (8)$$

The mode with the eigenvalue ε_n^\pm has the photon (atom) amplitude z_c^\pm (z_a^\pm). The energy levels of the ^{87}Rb atoms can be tuned by an external electrostatic field [55]. One example is shown in Fig. 1(b), namely, the variation of the two concerned Rydberg levels of ^{87}Rb with the electrostatic field [48]. This work considers the transition energy of ^{87}Rb , $\omega_n^a \in [\omega_1, \omega_2] \equiv [0.9\omega_0, 1.1\omega_0]$ where ω_1 and ω_2 correspond to the electrostatic fields of 544.2 and 542.6 V/cm, respectively. In experiments, such an electrostatic field on the n th JCE is controlled by the applied electric potential U_n , see Fig. 1(a). Apart from the two-level atoms, the energy spectra of some other two-level type emitters such as quantum dots can also be adjusted by the external electrostatic fields [56,57].

As for $H_{\text{JCE-bus}}$ and $H_{\text{JCE-branch}}$ [1,54], they can be written as

$$H_{\text{JCE-bus}} = \sum_{n=1}^N \int_{-\infty}^{\infty} dx V_0 \delta(x - x_n) \left[\hat{R}^\dagger(x) \hat{c}_n + \hat{L}^\dagger(x) \hat{c}_n + \text{h.c.} \right], \quad (9)$$

$$H_{\text{JCE-branch}} = \sum_{n=1}^N \int_0^{\infty} V_0 \delta(y) \left[\hat{U}_n^\dagger(y) \hat{c}_n + \text{h.c.} \right]. \quad (10)$$

The couplings of all cavities with the bus and branch waveguides are taken to be δ type [1,54,58] with identical strengths, i.e., $V_0 \delta(x - x_n)$ and $V_0 \delta(y)$, which are available as the non- δ -coupling effect can be neglected [59].

In order to investigate the transmission, reflection, and scattering properties, we start from the following single-particle wave function,

$$|\Phi\rangle = \sum_{n=1}^N \left[(\mathcal{C}_n \hat{c}_n^\dagger + \mathcal{A}_n \hat{\sigma}_n^+) + \int_0^{\infty} dy \mathcal{U}_n(y) \hat{U}_n^\dagger(y) \right] |\emptyset\rangle + \int_{-\infty}^{\infty} dx [\mathcal{R}(x) \hat{R}^\dagger(x) + \mathcal{L}(x) \hat{L}^\dagger(x)] |\emptyset\rangle. \quad (11)$$

Here, $|\emptyset\rangle$ represents the vacuum state, i.e., no photon in any waveguide or any cavity and all atoms are in their ground states. \mathcal{C}_n and \mathcal{A}_n represent the excitation amplitudes of the cavities and Rydberg atoms in the n th JCE, respectively. $\mathcal{R}(x)$ [$\mathcal{L}(x)$] is the wave function of the rightward-moving (leftward-moving) photon in the bus

waveguide and $\mathcal{U}_n(y)$ is the wave function of the upward-moving photon in the n th branch waveguide. Substituting Eqs. (1)–(4) and (9)–(11) into the eigenequation,

$$H |\Phi\rangle = \varepsilon |\Phi\rangle, \quad (12)$$

one can get the equation set,

$$\begin{aligned} \varepsilon \mathcal{R}(x) &= (\omega_0 - v_g k_0 - i v_g \partial_x) \mathcal{R}(x) \\ &+ \sum_{n=1}^N V_0 \delta(x - x_n) \mathcal{C}_n, \end{aligned} \quad (13a)$$

$$\begin{aligned} \varepsilon \mathcal{L}(x) &= (\omega_0 - v_g k_0 + i v_g \partial_x) \mathcal{L}(x) \\ &+ \sum_{n=1}^N V_0 \delta(x - x_n) \mathcal{C}_n, \end{aligned} \quad (13b)$$

$$\begin{aligned} \varepsilon \mathcal{C}_n &= \tilde{\omega}_n^c \mathcal{C}_n + \Omega \mathcal{A}_n \\ &+ V_0 [\mathcal{R}(x_n) + \mathcal{L}(x_n)] + V_0 \mathcal{U}_n(0), \end{aligned} \quad (13c)$$

$$\varepsilon \mathcal{A}_n = \tilde{\omega}_n^a \mathcal{A}_n + \Omega \mathcal{C}_n, \quad (13d)$$

$$\varepsilon \mathcal{U}_n(y) = (\omega_0 - v_g k_0 - i v_g \partial_y) \mathcal{U}_n(y) + V_0 \mathcal{C}_n \delta(y), \quad (13e)$$

for \mathcal{C}_n , \mathcal{A}_n , $\mathcal{R}(x)$, $\mathcal{L}(x)$, and $\mathcal{U}_n(y)$. Here, ε represents the energy of the incident photon. The waves in the bus and branch waveguides have the forms [54]

$$\begin{aligned} \mathcal{L}(x) &= e^{-ikx} \left[r_0 \theta(x_1 - x) + r_N \theta(x - x_N) \right. \\ &\left. + \sum_{n=1}^{N-1} r_n \theta(x - x_n) \theta(x_{n+1} - x) \right], \end{aligned} \quad (14a)$$

$$\begin{aligned} \mathcal{R}(x) &= e^{ikx} \left[t_0 \theta(x_1 - x) + t_N \theta(x - x_N) \right. \\ &\left. + \sum_{n=1}^{N-1} t_n \theta(x - x_n) \theta(x_{n+1} - x) \right], \end{aligned} \quad (14b)$$

$$\mathcal{U}_n(y) = e^{iky} \chi_n \theta(y), \quad (14c)$$

where $\theta(x)$ is the unit step function. t_n , r_n , and χ_n denote the amplitudes of the transmission, reflection, and scattering in the system, respectively, see Fig. 1(a).

Substituting Eq. (14) into Eq. (13), we can finally arrive at the following equations:

$$t_n = t_{n-1} + \frac{V_0}{iv_g} e^{-ikx_n} \mathcal{C}_n, \quad (15a)$$

$$r_n = r_{n-1} - \frac{V_0}{iv_g} e^{ikx_n} \mathcal{C}_n, \quad (15b)$$

$$\chi_n = \frac{V_0}{iv_g} \mathcal{C}_n, \quad (15c)$$

$$\mathcal{C}_n = V_0 \frac{(t_n + t_{n-1}) e^{ikx_n} + \chi_n + (r_n + r_{n-1}) e^{-ikx_n}}{2 \left(\varepsilon - \omega_n^c + i \gamma_n^c - \frac{\Omega^2}{\varepsilon - \omega_n^a + i \gamma_n^a} \right)}, \quad (15d)$$

where $n = 1, 2, \dots, N$ and \mathcal{C}_n is the excitation amplitude in the n th cavity. Since t_0 and r_N are known for a specific problem, the transmissivity, reflectivity, and scattering probabilities can be obtained by

$$T = |t_N|^2, \quad R = |r_0|^2, \quad S_n = |\chi_n|^2. \quad (16)$$

Hereafter, we focus on the scattering spectra S_n in this work to show the routing of the system.

III. NUMERICAL RESULT AND DISCUSSION

This section is divided into two subsections to show why the large-detuning mechanism of the JCEs can lead to a multichannel adjustable SP router. The two-level atoms are neglected ($\Omega = 0$) in Sec. III A, while are considered ($\Omega \neq 0$) in Sec. III B. In this section, the bus waveguide is considered to be infinite length and the parameters of $t_0 = 1$ and $r_N = 0$ are adopted in calculation. For convenience, the loss influences of cavities and atoms are not taken into account in these two cases.

A. Without atoms ($\Omega = 0$)

This subsection starts from the simple and intuitive example that all JCEs are replaced by the cavities, that is, the effect of the two-level atoms is ignored (i.e., $\Omega = 0$). We see that such an example cannot overcome all the disadvantages summarized above for a quantum router, though it can rout SPs indeed.

Figures 2(a) and 2(b) show the three- and six-cavity cases, respectively, for which the cavity frequencies are set to $\omega_n^c = [0.94 + 0.06(n-1)]\omega_0$ ($n = 1, 2, 3$) and $\omega_n^c = [0.93 + 0.03(n-1)]\omega_0$ ($n = 1, 2, \dots, 6$). Obviously, each S_n has a scattering peak when $\varepsilon = \omega_n^c$ and tends to zero when ε is away from ω_n^c , implying that the SPs with frequency ω_n^c can only output from the n th-branch waveguide apart from the right of the bus waveguide. This phenomenon can be used to separate the SPs with different frequencies, serving as a quantum filter. Compared with the previously proposed quantum routers [28,45], such a design could realize multichannel routing by increasing more branch waveguides and cavities. The limit on the number of channels is mainly determined by the FWHM of S_n , being $3\sqrt{2}V$ ($V \equiv V_0^2/v_g$ hereafter). To make sure all S_n peaks do not interfere with each other, the mutual eigenfrequency differences between any two cavities had better be larger than $20V$ (about five times of $3\sqrt{2}V$). This criteria leads to the limit of approximately 10 for the number of the branch waveguides in the range of $[0.9, 1.1]\omega_0$ in Fig. 2.

Although multichannel routing in Fig. 2 is realized, the disadvantages listed above are not all overcome satisfactorily. On the one hand, the number of output channels (i.e., the number of branch waveguides) is not large enough. On the other hand, the routing path of the SPs with a certain

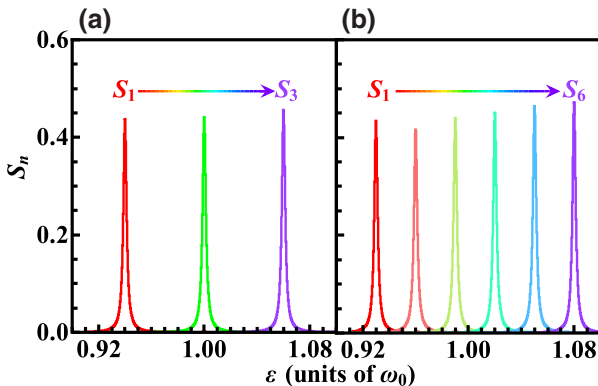


FIG. 2. Scattering spectra S_n for (a) the case with three cavities ($N = 3$) with $\omega_n^c = [0.94 + 0.06(n-1)]\omega_0$ ($n = 1, 2, 3$) and (b) the case with six cavities ($N = 6$) with $\omega_n^c = [0.93 + 0.03(n-1)]\omega_0$ ($n = 1, 2, \dots, 6$). Note that the two-level atoms are not considered in both cases. Other parameters: $d = 1.25\lambda_0$, $v_g = 0.5\omega_0/k_0$, $V \equiv V_0^2/v_g = 0.001\omega_0$, and $\gamma_n^c = 0$.

frequency cannot be changed in a settled structure, since the eigenfrequencies of cavities are commonly fixed once the cavities are fabricated. Accordingly, we turn to the following scheme, i.e., embedding a two-level atom into every cavity to form the JCE, see the following subsection.

B. With atoms ($\Omega \neq 0$)

Using the property that the transition energy of ^{87}Rb can be adjusted by an external electrostatic field [48], we can change ω_n^a in the range of $[0.9\omega_0, 1.1\omega_0]$. Eight output channels ($N = 8$) are considered as an example in Fig. 3. Figure 3(a) shows the tuning case, that is, $\omega_n^a \equiv \omega_n^c = [0.96 + 0.01(n-1)]\omega_0$ with $n = 1, 2, \dots, 8$, where there are two peaks for each S_n , located at $\varepsilon_n^\pm = \omega_n^a \pm \Omega$, referred to Eq. (6). The peaks in the left and right groups correspond to ε_n^- and ε_n^+ , respectively. Since the light from each branch waveguide has two energy centers, the system is not suitable to serve as a router in this case. Compared with Fig. 2, the peak widths in Fig. 3(a) almost do not change, implying an invariance of the number of channels acceptable in the frequency range of $[0.9\omega_0, 1.1\omega_0]$. In all, when the JCEs are in the tuning case, the system cannot work as a satisfactory router, similar to the case without atoms discussed in the last subsection.

However, when the JCEs work in the large detuning regime, that is, the detuning value $\Delta_n \equiv \omega_n^c - \omega_n^a \gg \Omega$, the peaks of S_n become very narrow, see Figs. 3(b) and 3(c) where all cavity eigenfrequencies are set to $\omega_n^c = 2\omega_0$ and thus $\Delta_n \approx \omega_0 \gg \Omega = 0.05\omega_0$. For $\omega_n^c = 2\omega_0$, the bonding states with ε_n^- are in the interested range of $[0.9\omega_0, 1.1\omega_0]$, while those antibonding ones with ε_n^+ are far away from ω_0 and thus can be neglected. The narrow widths of the S_n peaks in Figs. 3(b) and 3(c) mean that the light from the branch waveguide has a remarkable monochromaticity,

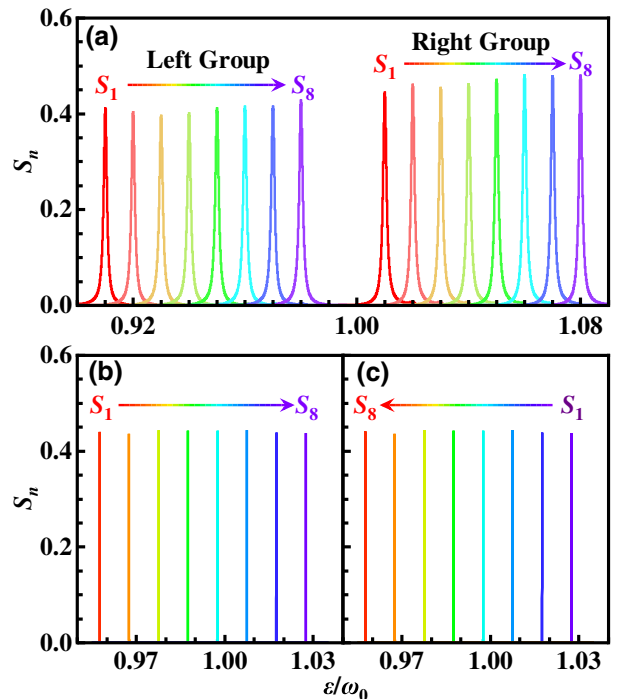


FIG. 3. Scattering spectra S_n for (a) the tuning case with $\omega_n^c \equiv \omega_n^a = [0.96 + 0.01(n-1)]\omega_0$ and (b, c) the large detuning cases with $\omega_n^c = 2\omega_0$ and $\omega_n^a = [0.96 + 0.01(n-1)]\omega_0$ in (b) and with $\omega_n^c = 2\omega_0$ and $\omega_n^a = [1.03 - 0.01(n-1)]\omega_0$ in (c), where $n = 1, 2, \dots, N$ with $N = 8$. Note that the two-level atoms are considered in all cases here. Other parameters: $d = 1.25\lambda_0$, $v_g = 0.5\omega_0/k_0$, $V \equiv V_0^2/v_g = 0.001\omega_0$, $\gamma_n^c = \gamma_n^a = 0$, and $\Omega = 0.05\omega_0$.

which can lead to a large number of channels acceptable in the range of $[0.9\omega_0, 1.1\omega_0]$.

Note that ω_n^c and ω_n^a are changed simultaneously in the tuning case of Fig. 3(a), while only ω_n^a is tuned in the large-detuning cases of Figs. 3(b) and 3(c). The latter brings us benefits because ω_n^c is mainly determined by the cavity geometry, not easy to be changed. For this reason, the design that all cavities of the JCEs are taken to be identical (with the same eigenfrequencies) not only benefits the fabrication of the structure in experiments but also permits researchers to choose the output channel for the photon as required. The way is to adjust the transition energy of each ^{87}Rb by an electrostatic field [48]. The examples with eight branch waveguides are provided in Figs. 3(b) and 3(c) where the transition energies of ^{87}Rb are set to $\omega_n^a = [0.96 + 0.01(n-1)]\omega_0$ and $\omega_n^a = [1.03 - 0.01(n-1)]\omega_0$, respectively, both corresponding to the branch waveguides from left to right in Fig. 1(a). The curves with the same color in Figs. 3(b) and 3(c) mean that the photon scattered into the n th-branch waveguide in Fig. 3(b) is routed to the $(9-n)$ th one in Fig. 3(c). Accordingly, the output channel of a photon in such a settled structure can be changed

merely by adjusting ω_n^a through an applied electrostatic field.

To find out how many branch waveguides we can place in the quantum router in the interested frequency range of $[0.9\omega_0, 1.1\omega_0]$, we investigate the relationship between the FWHM of the scattering peaks and ω_n^c (or Δ_n). For the case with only one JCE in the system, we plot the FWHM of S_1 as a function of the cavity eigenfrequency ω_c in Fig. 4(a). It is obvious that the FWHM sharply decreases with the increase of ω_c . Concretely speaking, the FWHM decreases from $1.5 \times 10^{-3}\omega_0$ to $7.5 \times 10^{-6}\omega_0$ ($1.9 \times 10^{-6}\omega_0$), about 200 (790) times, when ω_c moves from ω_0 to $2\omega_0$ ($3\omega_0$). This implies that the number of the branch waveguides can reach a very large value within a certain frequency window in the large detuning regime. The example provided in Fig. 4(b), with 2^{10} branch waveguides, takes $\omega_c = 2.3\omega_0$, corresponding to the FWHM of approximately $4.5 \times 10^{-6}\omega_0$. Due to the limited space, Fig. 4(b) presents an illusion that the scattering peaks are consecutive. To avoid this, 15 scattering spectra from S_{516} to S_{530} are enlarged in Fig. 4(c) for clear observation. In fact, we also confirm the feasibility of the case with 2^{11} branch waveguides by numerical calculation. The limit on the number of channels is determined by the FWHM of the scattering peak. If using the criteria that the frequency difference between the two adjacent scattering peaks is 10 times larger than the FWHM, one can get that more than 2^{12} channels could be accommodated in the frequency range of $[0.9\omega_0, 1.1\omega_0]$. This example proves that the architecture designed in Fig. 1(a) can work as the router with an amazing number of channels. Note that the disorder in waveguides may have an influence on the scattering peaks, particularly when the peaks are narrow. Fortunately, the topological waveguides have been proposed and studied in theory [60] and achieved in experiment [61], which can significantly depress the influence of disorders.

About this multichannel router, there are two questions that we should answer. One is why such a multichannel router requires the large detuning between the cavities and their corresponding embedded two-level atoms. The other is that the peak values of the scattering spectra are all about 0.44, see Figs. 3(b) and 3(c) and 4(b) and 4(c). To answer these two questions, we firstly substitute Eq. (15c) into Eq. (15d) to eliminate χ_n , then substitute C_n into Eqs. (15a)–(15c) to eliminate C_n , and finally obtain

$$t_n = t_{n-1} + \eta_n [(t_n + t_{n-1}) + (r_n + r_{n-1}) e^{-i2kx_n}], \quad (17a)$$

$$r_n = r_{n-1} - \eta_n [(t_n + t_{n-1}) e^{i2kx_n} + (r_n + r_{n-1})], \quad (17b)$$

$$\chi_n = \eta_n [e^{ikx_n} (t_n + t_{n-1}) + e^{-ikx_n} (r_n + r_{n-1})], \quad (17c)$$

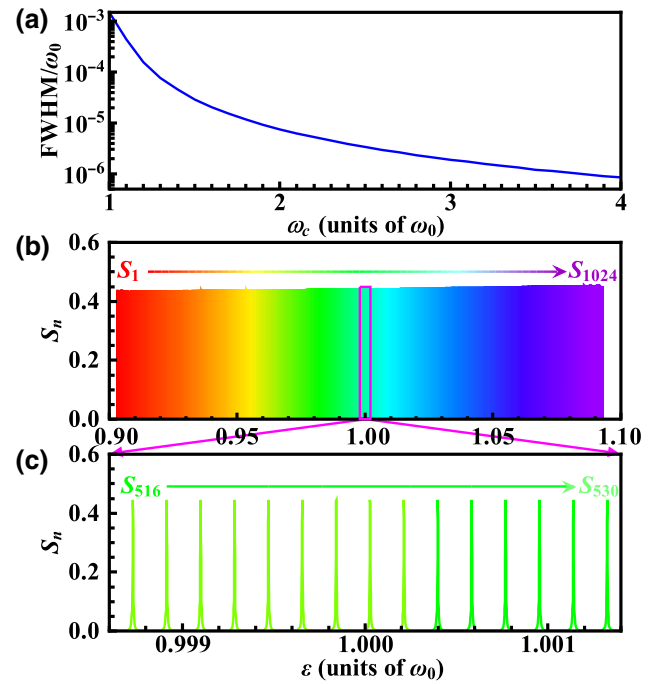


FIG. 4. (a) Variation of the FWHM of S_1 with ω_c^c in the case with only one JCE. Other parameters: $\omega_1^a = \omega_0$, $V = 0.001\omega_0$, $v_g = 0.5\omega_0/k_0$, $\gamma_1^c = \gamma_1^a = 0$, and $\Omega = 0.05\omega_0$. (b) Scattering spectra S_n for the large-detuning case with 2^{10} JCEs (i.e., $N = 2^{10}$), where $\omega_c^c = 2.3\omega_0$ and $\omega_n^a = [0.905 + 0.19/(N(n-1))] \omega_0$ with $n = 1, 2, \dots, N$. Other parameters: $V \equiv V_0^2/v_g = 0.001\omega_0$, $v_g = 0.5\omega_0/k_0$, $\Omega = 0.05\omega_0$, $d = 1.25\lambda_0$, and $\gamma_n^c = \gamma_n^a = 0$. (c) Enlarge of the part of (b) around the frequency ω_0 .

with

$$\eta_n = \frac{-iV}{2\xi_n + iV}, \quad \xi_n = \varepsilon - \tilde{\omega}_n^c - \frac{\Omega^2}{\varepsilon - \tilde{\omega}_n^a}. \quad (18)$$

Let us neglect the loss influence here. If $|\xi_n| \gg V$ we have $\eta_n \rightarrow 0$ and thus, all t_n tend to 1, implying all $S_n \rightarrow 0$ under this constraint. Because $|\xi_n|$ can be expanded as

$$|\xi_n| = |\varepsilon - \varepsilon_n^-| \frac{\Delta_n^2}{\Omega^2}, \quad (19)$$

at ε_n^- , the constraint of $|\xi_n| \gg V$ leads to the large detuning, $\Delta_n \gg \Omega$. That is, as the JCEs work in the large-detuning regime the scattering probability S_n tends to zero if the frequency of the incident photon ε is not equal to ε_n^- .

In contrast, when the frequency of the incident photon meets the level of the bonding state of the n th JCE, i.e., $\varepsilon = \varepsilon_m^-$ ($\varepsilon \neq \varepsilon_n^-$ for $n \neq m$), we can immediately find

$$t_n \approx t_0 \text{ and } r_n \approx r_0, \text{ when } n \leq m-1, \quad (20a)$$

$$t_n \approx t_N \text{ and } r_n \approx r_N, \text{ when } n \geq m. \quad (20b)$$

Since $\xi_m = 0$ when $\varepsilon = \varepsilon_m^-$, we have $\eta_m = -1$. Using this relation and substituting Eqs. (18) and (20) into Eq. (17), we can find T , R , and S_n as

$$T = \frac{1}{9}, \quad R = \frac{4}{9}, \quad S_n|_{n \neq m} = 0, \quad S_m = \frac{4}{9}. \quad (21)$$

Accordingly, the peak value of S_m is about 0.44. This conclusion is irrelevant to the value of V and thus ensures the availability of the router.

IV. DISCUSSION FOR APPLICATION

In view of application, there are some factors that may influence the work of the router. Here, three factors are considered, that is, the system losses, the interferential levels in atoms, and the way to increase the routing probability. According to them, this section is divided into three parts. We discuss the influence of the system losses in Sec. IV A, analyze the effects of the interferential levels in atoms in Sec. IV B, and demonstrate a technique to make the routing probability be able to reach 100% in Sec. IV C. The bus waveguide is also considered to be infinite length in Sec. IV A and Sec. IV B, for which $t_0 = 1$ and $r_N = 0$.

A. Influence of losses

On the influence of the system losses, the cavity losses almost do not influence the scattering spectra S_n when the JCEs work in the large detuning regime, i.e., $\Delta_n \gg \Omega$. The reason for this is that the photon component of the bonding state in each JCE (with the energy ε_n^-) is proportional to $|z_c^-|^2 \approx \frac{\Omega^2}{\Delta_n^2}$, much less than 1 when $\Delta_n \gg \Omega$. In contrast, the atom component approximates $|z_a^-|^2 \approx 1$, implying the strong influence of the atom losses on the scattering spectra. These arguments can be derived from Eqs. (5)–(8) by doing some algebraic simplification. To confirm these, we plot the scattering spectra with the losses of cavities and atoms in Fig. 5. For convenience, we set all γ_n^c (γ_n^a) equal to each other, i.e., $\gamma_n^c \equiv \gamma_c$ ($\gamma_n^a \equiv \gamma_a$). From Figs. 5(a) and 5(b), we can see that the peak values decrease significantly with the increase of γ_a . However, Figs. 5(c) and 5(d) show that the peak values almost do not decrease as γ_c increases. As a result, the system is not sensitive to the cavity losses and the major influence of losses is from the atoms. Fortunately, the loss rate of Rydberg atoms can be less than 10^4 Hz [62], about $10^{-6}\omega_0$ here. Figure 5(a) shows that the peak values are larger than 0.25 when $\gamma_a = 10^{-6}\omega_0$, which is acceptable for a practical router. To summarize, the large detuning can depress the influence of the cavity losses. When $\gamma_n^a = 10^{-6}\omega_0$ is taken, all scattering spectra keep the line form, only with a little decrease of the peak values, indicating that the router is feasible.

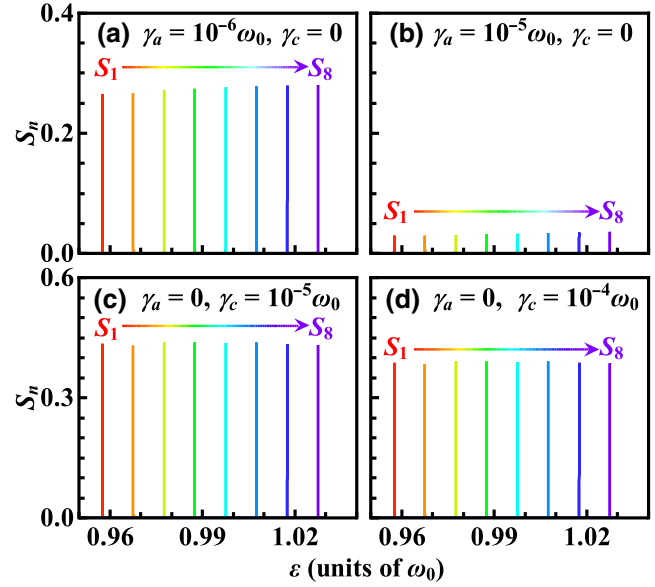


FIG. 5. Scattering spectra S_n under different losses. In (a) $\gamma_a = 10^{-6}\omega_0$ and $\gamma_c = 0$; in (b) $\gamma_a = 10^{-5}\omega_0$ and $\gamma_c = 0$; in (c) $\gamma_a = 0$ and $\gamma_c = 10^{-5}\omega_0$; and in (d) $\gamma_a = 0$, $\gamma_c = 10^{-4}\omega_0$. Other parameters: $\omega_n^c = 2\omega_0$, $\omega_n^a = 0.96 + 0.01(n-1)\omega_0$ ($n = 1, 2, \dots, 8$), $d = 1.25\lambda_0$, $v_g = 0.5\omega_0/k_0$, $V \equiv V_0^2/v_g = 0.001\omega_0$, and $\Omega = 0.05\omega_0$.

B. Influence of interferential levels in atoms

In the Rydberg atoms, there are plenty of energy levels. When we consider the detuning transitions of the Rydberg atoms (with respect to the cavity modes), there may exist the tuning transitions that couple to the cavity modes. Are these interferential tuning transitions harmful to the performance of the suggested router? This section takes the V- and Λ -type atoms [63,64] as examples to explore this question, see Figs. 6(a) and 6(b). The V-type atom shares the same ground state $|g\rangle$ with two excited states $|e_a\rangle$ and $|e_i\rangle$. The transition energy between $|e_a\rangle$ and $|g\rangle$ equals ω_n^a , the same as that in the two-level atom used in Figs. 3 and 4. The transition energy between $|e_i\rangle$ and $|g\rangle$ is denoted as ω_n^i , taken as the interferential term. For the Λ -type atom, it has two ground states $|g_a\rangle$ and $|g_i\rangle$ with one excited state $|e\rangle$. The interferential term is the transition between the $|g_i\rangle$ and $|e\rangle$. The transition energy between $|g_a\rangle$ and $|e\rangle$ equals that in the two-level atom, i.e., ω_n^a .

The coupling between each of these two types of atoms with the cavity leads to a quantum emitter like the JCE. The two corresponding quantum emitters have the same Hamiltonian [65],

$$H_{\text{emitter}} = \sum_{n=1}^N \left[(\omega_n^c \hat{c}_n^\dagger \hat{c}_n + \omega_n^a \hat{\sigma}_n^{a+} \hat{\sigma}_n^{a-} + \omega_n^i \hat{\sigma}_n^{i+} \hat{\sigma}_n^{i-}) + \Omega (\hat{c}_n^\dagger \hat{\sigma}_n^{a-} + \hat{c}_n^\dagger \hat{\sigma}_n^{i-} + \text{h.c.}) \right], \quad (22)$$

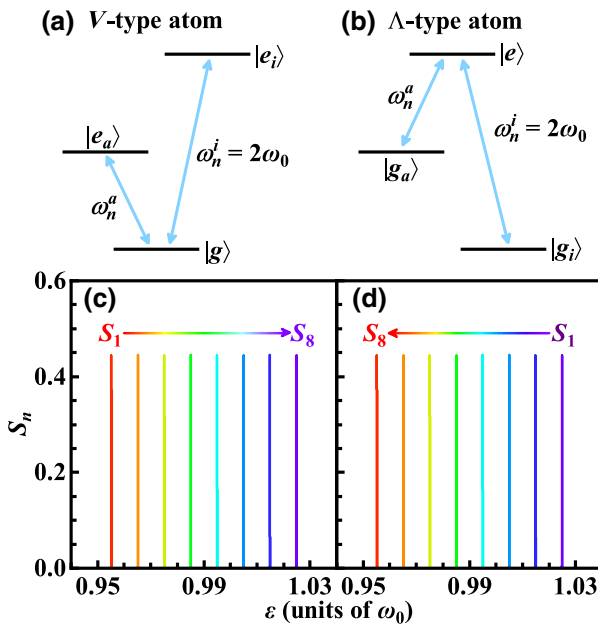


FIG. 6. Energy-level schematic diagrams for the V-type (a) and Λ -type (b) atoms in the n th quantum emitter. Both of them have three energy levels and two transition energies (ω_n^a and ω_n^i). (c),(d) are the scattering spectra S_n . In (c) $\omega_n^a = [0.96 + 0.01(n-1)]\omega_0$ and in (d) $\omega_n^a = [1.03 - 0.01(n-1)]\omega_0$, where $n = 1, 2, \dots, N$ with $N = 8$. Other parameters: $\omega_n^i = \omega_n^c = 2\omega_0$, $d = 1.25\lambda_0$, $v_g = 0.5\omega_0/k_0$, $V \equiv V_0^2/v_g = 0.001\omega_0$, and $\Omega = 0.05\omega_0$.

where \hat{c}_n^{a-} and \hat{c}_n^{a+} ($\hat{\sigma}_n^{i-}$ and $\hat{\sigma}_n^{i+}$), respectively, represent the lowering and raising operators between the two levels with the transition energy ω_n^a (ω_n^i), see Figs. 6(a) and 6(b). Without loss of generality, we assume that like in Sec. II, ω_n^a can be adjusted in the range of $[0.9\omega_0, 1.1\omega_0]$ and ω_n^i is always settled to be $\omega_n^i \equiv \omega_n^c = 2\omega_0$. Apart from the quantum emitters, the Hamiltonians of the other parts in the whole system are identical to those described in Sec. II. However, the single-particle state should be changed into

$$|\Phi\rangle = \sum_{n=1}^N \left[(\mathcal{C}_n \hat{c}_n^\dagger + \mathcal{A}_n^a \hat{\sigma}_n^{a+} + \mathcal{A}_n^i \hat{\sigma}_n^{i+}) + \int_0^\infty dy \mathcal{U}_n(y) \hat{U}_n^\dagger(y) \right] |\emptyset\rangle + \int_{-\infty}^\infty dx [\mathcal{R}(x) \hat{R}^\dagger(x) + \mathcal{L}(x) \hat{L}^\dagger(x)] |\emptyset\rangle, \quad (23)$$

where \mathcal{A}_n^a (\mathcal{A}_n^i) represents the excitation amplitude of the three-level atom corresponding to ω_n^a (ω_n^i) in the n th quantum emitter. Using the same method in Sec. II, we can get the equation set for \mathcal{C}_n , \mathcal{A}_n^a , \mathcal{A}_n^i , $\mathcal{R}(x)$, $\mathcal{L}(x)$, and $\mathcal{U}_n(y)$ as

follows:

$$\begin{aligned} \varepsilon \mathcal{R}(x) &= (\omega_0 - v_g k_0 - i v_g \partial_x) \mathcal{R}(x) \\ &+ \sum_{n=1}^N V_0 \delta(x - x_n) \mathcal{C}_n, \end{aligned} \quad (24a)$$

$$\begin{aligned} \varepsilon \mathcal{L}(x) &= (\omega_0 - v_g k_0 + i v_g \partial_x) \mathcal{L}(x) \\ &+ \sum_{n=1}^N V_0 \delta(x - x_n) \mathcal{C}_n, \end{aligned} \quad (24b)$$

$$\begin{aligned} \varepsilon \mathcal{C}_n &= \omega_n^c \mathcal{C}_n + \Omega (\mathcal{A}_n^a + \mathcal{A}_n^i) \\ &+ V_0 [\mathcal{R}(x_n) + \mathcal{L}(x_n)] + V_0 \mathcal{U}(0), \end{aligned} \quad (24c)$$

$$\varepsilon \mathcal{A}_n^a = \omega_n^a \mathcal{A}_n^a + \Omega \mathcal{C}_n, \quad (24d)$$

$$\varepsilon \mathcal{A}_n^i = \omega_n^i \mathcal{A}_n^i + \Omega \mathcal{C}_n, \quad (24e)$$

$$\varepsilon \mathcal{U}_n(y) = (\omega_0 - v_g k_0 - i v_g \partial_y) \mathcal{U}_n(y) + V_0 \mathcal{C}_n \delta(y). \quad (24f)$$

Further, substituting the wave functions in Eq. (14) into Eq. (24) yields

$$t_n = t_{n-1} + \eta'_n [(t_n + t_{n-1}) + (r_n + r_{n-1}) e^{-i2kx_n}], \quad (25a)$$

$$r_n = r_{n-1} - \eta'_n [(t_n + t_{n-1}) e^{i2kx_n} + (r_n + r_{n-1})], \quad (25b)$$

$$\chi_n = \eta'_n [e^{ikx_n} (t_n + t_{n-1}) + e^{-ikx_n} (r_n + r_{n-1})], \quad (25c)$$

with

$$\eta'_n = \frac{-iV}{2\xi'_n + iV}, \quad (26)$$

$$\xi'_n = \varepsilon - \omega_n^c - \frac{\Omega^2 [(\varepsilon - \omega_n^a) + (\varepsilon - \omega_n^i)]}{(\varepsilon - \omega_n^a)(\varepsilon - \omega_n^i)}. \quad (27)$$

Using Eq. (25), one can calculate the scattering spectra $S_n \equiv |\chi_n|^2$ for the cavities with the three-level atoms, see Fig. 6(c) where eight channels are taken as an example. In Fig. 6(c), we set $\omega_n^a = [0.96 + 0.01(n-1)]\omega_0$ with $n = 1, 2, \dots, 8$. If we reversely set $\omega_n^a = [1.03 - 0.01(n-1)]\omega_0$, the output channel for a certain photon will be changed, comparing Fig. 6(d) with Fig. 6(c). The curves with the same color mean that the photon scattered into the n th-branch waveguide in Fig. 6(c) is routed to the $(9-n)$ th one in Fig. 6(d). Accordingly, the interferential levels show a negligible influence on the router, even when their corresponding transitions are tuned to the cavity mode. Note that this is also because the quantum emitters work in the large detuning regime.

C. Increasing routing probability

High routing efficiency is vital for a quantum router in application. The SP router discussed above has the routing probability of less than 0.5 in theory. Can all the routing probabilities S_n be improved to approximately 100%? Equation (21) implies that the loss of routing probability is due to nonzero R and T . This suggests us to refit the SP router by adding a mirror and a phase shifter [66] to the right terminal of the bus waveguide, see Fig. 7(a). The rightward-moving SP can be reflected completely when it meets the mirror, leading to $|r_N| = |t_N|$. After taking the induced phase δ into account, we can write down $r_N = t_N e^{i\delta}$. This refit can increase the routing probability to approximately 100% by tuning δ .

Owing to $r_N \neq 0$, the peak position of S_n is no longer at ε_n^- strictly and has a small deviation from it with a magnitude V (see later). For convenience, we denote the peak position of S_n as E_n . Because E_n approximates ε_n^- , the analysis for Eq. (20) is also available for analyzing

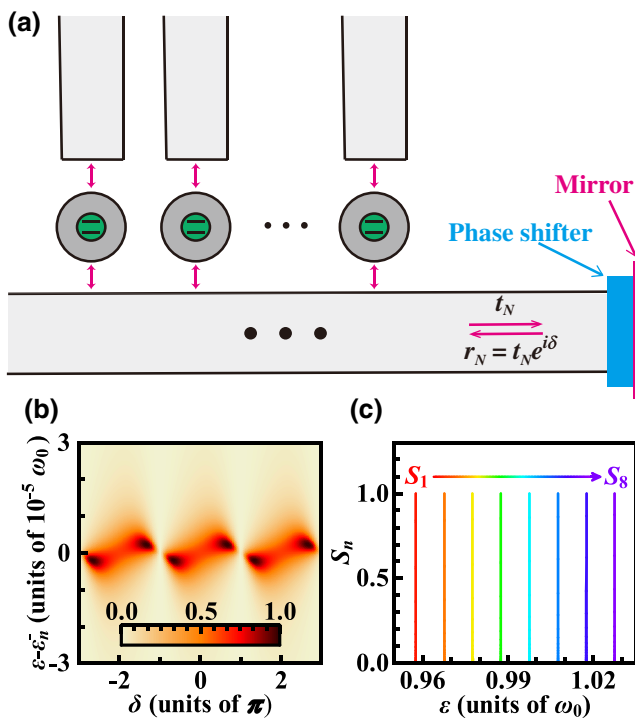


FIG. 7. (a) Schematic diagram of the refitted structure by adding a mirror and a phase shifter to the end of the bus waveguide. The mirror can reflect the rightward-moving wave completely. The phase shifter brings a phase shift δ to the reflected wave, i.e., $r_N = t_N e^{i\delta}$. (b) Variation of S_1 with the SP frequency ε and the phase δ , for which only one branch waveguide is considered. Parameters: $\omega_1^a = \omega_0$, $\omega_1^c = 2\omega_0$, $x_1 = 0$. (c) Scattering peaks S_n for $\omega_n^a = [0.96 + 0.01(n-1)]\omega_0$, $\omega_n^c = 2\omega_0$, and $\delta = \delta_n^+$, with $n = 1, 2, \dots, 8$. Other parameters: $d = 1.25\lambda_0$, $v_g = 0.5\omega_0/k_0$, $V \equiv V_0^2/v_g = 0.001\omega_0$, $\gamma_1^a = \gamma_1^c = 0$, and $\Omega = 0.05\omega_0$.

the transmission and reflection coefficients, t_n and r_n , if the incident photon has the frequency $\varepsilon = E_m$. That is, Eq. (20) also works for $\varepsilon = E_m$. Combining $t_0 = 1$ and $r_N = t_N e^{i\delta}$, we can find

$$r_0|_{\varepsilon=E_m} = \frac{2\eta_1 + (1+2\eta_1)e^{i(\delta-2kx_m)}}{(1-2\eta_1)-2\eta_1 e^{i(\delta-2kx_m)}} e^{i2kx_m}. \quad (28)$$

Because there is no leak of the SP at the right terminal of the bus waveguide, one can expect $S_m|_{\varepsilon=E_m} = 100\%$ when $r_0|_{\varepsilon=E_m} = 0$, which leads to

$$\delta = \delta_m^\pm \equiv 2kx_m \pm \frac{2\pi}{3} + 2j\pi, \quad (29)$$

$$\xi_m = \pm \frac{\sqrt{3}}{2}V. \quad (30)$$

There are two possible values δ_m^\pm for the phase δ if the integral multiple of 2π is neglected. The corresponding two E_m (E_m^\pm) are determined by Eq. (29),

$$E_m^\pm \approx \varepsilon_m^- \pm \frac{\sqrt{3}}{2} \frac{\Omega^2}{\Delta_m^2} V. \quad (31)$$

Accordingly, one can expect the routing probability $S_m \approx 100\%$ at $\varepsilon = E_m^\pm$ when setting $\delta = \delta_m^\pm$, respectively.

To verify this analysis, the case with only one channel located at $x = 0$ is studied in Fig. 7(b) where the routing probability S_1 is plotted as a function of the phase δ and the energy deviation $\varepsilon - \varepsilon_1^-$. The routing probability S_1 has two positions in energy to approach 100% and presents periodical variation with the phase. Accordingly, it is in practice to improve the routing probability by adding a mirror and a phase shifter to the right terminal of the bus waveguide. Such a refit for the case with eight channels is shown in Fig. 7(c). The peak values of all scattering spectra can reach 100% now. These two examples confirm the effectiveness of the refitting technique.

Photons are a kind of ideal carrier in the long-distance transport of quantum information, since they not only have no direct mutual influence but also commonly show a very weak interaction with environment. The intuitive and useful application of the proposed router is to distribute the photons carrying information. Let us consider that the information is encoded into the photon momentum. Due to the one-to-one relationship between momentum and energy, the incident SPs, carrying different momentum in the bus waveguide, would be routed to different channels, so that information separation is achieved for subsequent processing.

V. CONCLUSION

To summarize, this work suggests an adjustable multichannel SP router based on one-dimensional bus

waveguide coupled to numerous JCEs. Each JCE contains a Rydberg atom ^{87}Rb and terminally couples to a semi-infinite branch waveguide as an output channel. The Rydberg levels of the atom ^{87}Rb can be tuned conveniently by an external electrostatic field, responsible for the adjustability of the router. We prove that the large-detuning mechanism of the JCEs can improve the performance of the SP router. Firstly, the number of channels can reach more than a thousand. Secondly, the routing channel for a certain photon can be adjusted on demand. Thirdly, each routing channel has a very narrow peak in the spectra. Fourthly, the influence of cavity losses can be depressed by the large-detuning mechanism, which benefits the fabrication of the optical architecture. In addition, the large detuning can also avoid the influence of interferential levels in atoms. Moreover, the routing probability can reach approximately 100% by adding a mirror and a phase shifter to the end of the bus waveguide. These merits enable the suggested SP router to have a significant potential in quantum informatics.

ACKNOWLEDGMENT

This work is supported by National Natural Science Foundation of China (Grant No. 12074037) and Bagui scholar fund of Guangxi province. The authors would like to thank Professor Xiangdong Zhang for helpful conversations and Yuhong He for improving the language.

- [1] J.-T. Shen and S. Fan, Theory of single-photon transport in a single-mode waveguide. I. Coupling to a cavity containing a two-level atom, *Phys. Rev. A* **79**, 023837 (2009).
- [2] D. Englund, A. Majumdar, A. Faraon, M. Toishi, N. Stoltz, P. Petroff, and J. Vučković, Resonant Excitation of a Quantum Dot Strongly Coupled to a Photonic Crystal Nanocavity, *Phys. Rev. Lett.* **104**, 073904 (2010).
- [3] A. Laucht, S. Pütz, T. Günthner, N. Hauke, R. Saive, S. Frédéric, M. Bichler, M.-C. Amann, A. W. Holleitner, M. Kaniber, and J. J. Finley, A Waveguide-Coupled On-Chip Single-Photon Source, *Phys. Rev. X* **2**, 011014 (2012).
- [4] J.-F. Huang, T. Shi, C. P. Sun, and F. Nori, Controlling single-photon transport in waveguides with finite cross section, *Phys. Rev. A* **88**, 013836 (2013).
- [5] J. F. M. Werra, P. Longo, and K. Busch, Spectra of coherent resonant light pulses interacting with a two-level atom in a waveguide, *Phys. Rev. A* **87**, 063821 (2013).
- [6] X. Zang and C. Jiang, Single-photon transport properties in a waveguide–cavity system, *J. Phys. B: At., Mol. Opt. Phys.* **43**, 065505 (2010).
- [7] J. Minář, Š. G. Söyler, and I. Lesanovsky, Non-equilibrium dynamics of a nonlinear Jaynes–Cummings model in cavity arrays, *New J. Phys.* **18**, 053035 (2016).
- [8] J.-Q. Liao and C. K. Law, Correlated two-photon transport in a one-dimensional waveguide side-coupled to a nonlinear cavity, *Phys. Rev. A* **82**, 053836 (2010).

- [9] M. Klein, M. Hohensee, Y. Xiao, R. Kalra, D. F. Phillips, and R. L. Walsworth, Slow-light dynamics from electromagnetically-induced-transparency spectra, *Phys. Rev. A* **79**, 053833 (2009).
- [10] R. D. Kekatpure, E. S. Barnard, W. Cai, and M. L. Brongersma, Phase-Coupled Plasmon-Induced Transparency, *Phys. Rev. Lett.* **104**, 243902 (2010).
- [11] K. Kobayashi, H. Aikawa, A. Sano, S. Katsumoto, and Y. Iye, Fano resonance in a quantum wire with a side-coupled quantum dot, *Phys. Rev. B* **70**, 035319 (2004).
- [12] S. Hayashi, D. V. Nesterenko, and Z. Sekkat, Fano resonance and plasmon-induced transparency in waveguide-coupled surface plasmon resonance sensors, *Appl. Phys. Exp.* **8**, 022201 (2015).
- [13] D. O’Shea, C. Junge, J. Volz, and A. Rauschenbeutel, Fiber-Optical Switch Controlled by a Single Atom, *Phys. Rev. Lett.* **111**, 193601 (2013).
- [14] T. Shi and S. Fan, Two-photon transport through a waveguide coupling to a whispering-gallery resonator containing an atom and photon-blockade effect, *Phys. Rev. A* **87**, 063818 (2013).
- [15] S. Xu, E. Rephaeli, and S. Fan, Analytic Properties of Two-Photon Scattering Matrix in Integrated Quantum Systems Determined by the Cluster Decomposition Principle, *Phys. Rev. Lett.* **111**, 223602 (2013).
- [16] L. Li, C. Liu, and Q.-H. Wang, Optical switch based on tunable aperture, *Opt. Lett.* **37**, 3306 (2012).
- [17] Q. Jiang, Q. Hu, B. Zou, and Y. Zhang, Single microwave photon switch controlled by an external electrostatic field, *Phys. Rev. A* **98**, 023830 (2018).
- [18] I.-C. Hoi, A. F. Kockum, T. Palomaki, T. M. Stace, B. Fan, L. Tornberg, S. R. Sathyamoorthy, G. Johansson, P. Delsing, and C. M. Wilson, Giant Cross–Kerr Effect for Propagating Microwaves Induced by an Artificial Atom, *Phys. Rev. Lett.* **111**, 053601 (2013).
- [19] J. Sprengers, A. Gaggero, D. Sahin, S. Jahanmirinejad, G. Frucci, F. Mattioli, R. Leoni, J. Beetz, M. Lermer, and M. Kamp, Waveguide superconducting single-photon detectors for integrated quantum photonic circuits, *Appl. Phys. Lett.* **99**, 181110 (2011).
- [20] H. Gorniaczyk, C. Tresp, J. Schmidt, H. Fedder, and S. Hofferberth, Single-Photon Transistor Mediated by Inter-state Rydberg Interactions, *Phys. Rev. Lett.* **113**, 053601 (2014).
- [21] K. F. Reim, P. Michelberger, K. C. Lee, J. Nunn, N. K. Langford, and I. A. Walmsley, Single-Photon-Level Quantum Memory at Room Temperature, *Phys. Rev. Lett.* **107**, 053603 (2011).
- [22] J. Pan, Y. Huo, S. Sandhu, N. Stuurmann, M. L. Povinelli, J. S. Harris, M. Fejer, and S. Fan, Tuning the coherent interaction in an on-chip photonic-crystal waveguide-resonator system, *Appl. Phys. Lett.* **97**, 101102 (2010).
- [23] D. Roy, Cascaded two-photon nonlinearity in a one-dimensional waveguide with multiple two-level emitters, *Sci. Rep.* **3**, 2337 (2013).
- [24] Y.-L. L. Fang, H. Zheng, and H. U. Baranger, One-dimensional waveguide coupled to multiple qubits: photon–photon correlations, *EPJ Quantum Technol.* **1**, 3 (2014).
- [25] K. Lemr, K. Bartkiewicz, A. Černoch, and J. Soubusta, Resource-efficient linear-optical quantum router, *Phys. Rev. A* **87**, 062333 (2013).

- [26] Z. Wang, Y. Wu, Z. Bao, Y. Li, C. Ma, H. Wang, Y. Song, H. Zhang, and L. Duan, Experimental Realization of a Deterministic Quantum Router with Superconducting Quantum Circuits, *Phys. Rev. Appl.* **15**, 014049 (2021).
- [27] L. Zhou, L.-P. Yang, Y. Li, and C. P. Sun, Quantum Routing of Single Photons with a Cyclic Three-Level System, *Phys. Rev. Lett.* **111**, 103604 (2013).
- [28] M. Ahumada, P. A. Orellana, F. Domínguez-Adame, and A. V. Malyshev, Tunable single-photon quantum router, *Phys. Rev. A* **99**, 033827 (2019).
- [29] M. Ahumada, P. A. Orellana, and A. V. Malyshev, Manipulating photonic signals by a multipurpose quantum junction, *Phys. Rev. A* **105**, 043502 (2022).
- [30] I.-C. Hoi, C. M. Wilson, G. Johansson, T. Palomaki, B. Peropadre, and P. Delsing, Demonstration of a Single-Photon Router in the Microwave Regime, *Phys. Rev. Lett.* **107**, 073601 (2011).
- [31] X. Gu, A. F. Kockum, A. Miranowicz, Y.-x. Liu, and F. Nori, Microwave photonics with superconducting quantum circuits, *Phys. Rep.* **718-719**, 1 (2017).
- [32] T. Aoki, A. S. Parkins, D. J. Alton, C. A. Regal, B. Dayan, E. Ostby, K. J. Vahala, and H. J. Kimble, Efficient Routing of Single Photons by One Atom and a Microtoroidal Cavity, *Phys. Rev. Lett.* **102**, 083601 (2009).
- [33] L. Zhou, Z. R. Gong, Y.-x. Liu, C. P. Sun, and F. Nori, Controllable Scattering of a Single Photon inside a One-Dimensional Resonator Waveguide, *Phys. Rev. Lett.* **101**, 100501 (2008).
- [34] J.-Q. Liao, Z. R. Gong, L. Zhou, Y.-x. Liu, C. P. Sun, and F. Nori, Controlling the transport of single photons by tuning the frequency of either one or two cavities in an array of coupled cavities, *Phys. Rev. A* **81**, 042304 (2010).
- [35] J. Lu, L. Zhou, L.-M. Kuang, and F. Nori, Single-photon router: Coherent control of multichannel scattering for single photons with quantum interferences, *Phys. Rev. A* **89**, 013805 (2014).
- [36] W.-B. Yan and H. Fan, Single-photon quantum router with multiple output ports, *Sci. Rep.* **4**, 4820 (2014).
- [37] W.-B. Yan and H. Fan, Control of single-photon transport in a one-dimensional waveguide by a single photon, *Phys. Rev. A* **90**, 053807 (2014).
- [38] W. Qin and F. Nori, Controllable single-photon transport between remote coupled-cavity arrays, *Phys. Rev. A* **93**, 032337 (2016).
- [39] B. K. Behera, T. Reza, A. Gupta, and P. K. Panigrahi, Designing quantum router in IBM quantum computer, *Quantum Inf. Process.* **18**, 328 (2019).
- [40] J.-S. Huang, J.-H. Zhang, and L.-F. Wei, Quantum routing of surface plasmons by two quantum dots, *J. Mod. Opt.* **66**, 958 (2019).
- [41] Y. T. Zhu and W. Z. Jia, Single-photon quantum router in the microwave regime utilizing double superconducting resonators with tunable coupling, *Phys. Rev. A* **99**, 063815 (2019).
- [42] B. Poudyal and I. M. Mirza, Collective photon routing improvement in a dissipative quantum emitter chain strongly coupled to a chiral waveguide QED ladder, *Phys. Rev. Res.* **2**, 043048 (2020).
- [43] Y.-J. Zhao, N. Tan, D. Yu, B. Liu, and W.-M. Liu, Tunable quantum switcher and router of single atoms using localized artificial magnetic fields, *Phys. Rev. Res.* **2**, 033484 (2020).
- [44] X.-P. Du, Q. Cao, N. Dang, and L. Tan, Quantum router modulated by two Rydberg atoms in a X-shaped coupled cavity array, *Eur. Phys. J. D* **75**, 79 (2021).
- [45] D.-C. Yang, M.-T. Cheng, X.-S. Ma, J. Xu, C. Zhu, and X.-S. Huang, Phase-modulated single-photon router, *Phys. Rev. A* **98**, 063809 (2018).
- [46] J.-S. Huang, J.-W. Wang, Y. Wang, Z.-H. Xu, and Y.-W. Zhong, Single-photon routing in a multi-t-shaped waveguide, *J. Phys. B: At., Mol. Opt. Phys.* **52**, 015502 (2018).
- [47] X. Li, J. Xin, G. Li, X.-M. Lu, and L. F. Wei, Quantum routings for single photons with different frequencies, *Opt. Exp.* **29**, 8861 (2021).
- [48] D. Yu, A. Landra, M. M. Valado, C. Hufnagel, L. C. Kwek, L. Amico, and R. Dumke, Superconducting resonator and Rydberg atom hybrid system in the strong coupling regime, *Phys. Rev. A* **94**, 062301 (2016).
- [49] C.-Y. Chen, X.-L. Zhang, Z. J. Deng, K.-L. Gao, and M. Feng, Influence from cavity decay on geometric quantum computation in the large-detuning cavity QED model, *Phys. Rev. A* **74**, 032328 (2006).
- [50] P. Orellana, M. L. de Guevara, and F. Domínguez-Adame, Electronic transmission through a quantum wire by side-attached nanowires, *Phys. E* **25**, 384 (2005).
- [51] J. D. Hood, A. Goban, A. Asenjo-Garcia, M. Lu, S.-P. Yu, D. E. Chang, and H. Kimble, Atom-atom interactions around the band edge of a photonic crystal waveguide, *Proc. Natl. Acad. Sci.* **113**, 10507 (2016).
- [52] T. Yoshie, A. Scherer, J. Hendrickson, G. Khitrova, H. Gibbs, G. Rupper, C. Ell, O. Shchekin, and D. Deppe, Vacuum Rabi splitting with a single quantum dot in a photonic crystal nanocavity, *Nature* **432**, 200 (2004).
- [53] M. Mucke, E. Figueroa, J. Bochmann, C. Hahn, K. Murr, S. Ritter, C. J. Villas-Boas, and G. Rempe, Electromagnetically induced transparency with single atoms in a cavity, *Nature* **465**, 755 (2010).
- [54] J. Dong, Q. Jiang, Q. Hu, B. Zou, and Y. Zhang, Transport and entanglement for single photons in optical waveguide ladders, *Phys. Rev. A* **100**, 013840 (2019).
- [55] C. S. Adams, J. D. Pritchard, and J. P. Shaffer, Rydberg atom quantum technologies, *J. Phys. B: At. Mol. Opt. Phys.* **53**, 012002 (2019).
- [56] J. Dreiser, M. Atatüre, C. Galland, T. Müller, A. Badolato, and A. Imamoglu, Optical investigations of quantum dot spin dynamics as a function of external electric and magnetic fields, *Phys. Rev. B* **77**, 075317 (2008).
- [57] W. Xie, Impurity effects on optical property of a spherical quantum dot in the presence of an electric field, *Phys. B* **405**, 3436 (2010).
- [58] Y. Wang, Y. Zhang, Q. Zhang, B. Zou, and U. Schwengenschlogl, Dynamics of single photon transport in a one-dimensional waveguide two-point coupled with a Jaynes-Cummings system, *Sci. Rep.* **6**, 33867 (2016).
- [59] Y. Zhang and B. Zou, Effects of non- δ coupling between one-dimensional waveguides and side optical cavities, *Phys. Rev. A* **89**, 063815 (2014).
- [60] J. Dong, B. Zou, and Y. Zhang, Theoretical study of transparent peaks in a topological waveguide-cavity coupled system, *Appl. Phys. Lett.* **119**, 251101 (2021).

- [61] S. Iwamoto, Y. Ota, and Y. Arakawa, Recent progress in topological waveguides and nanocavities in a semiconductor photonic crystal platform, *Opt. Mater. Exp.* **11**, 319 (2021).
- [62] I. I. Beterov, I. I. Ryabtsev, D. B. Tretyakov, and V. M. Entin, Quasiclassical calculations of blackbody-radiation-induced depopulation rates and effective lifetimes of Rydberg nS , nP , and nD alkali-metal atoms with $n \leq 80$, *Phys. Rev. A* **79**, 052504 (2009).
- [63] N.-C. Kim, M.-C. Ko, and C.-I. Choe, Scattering of a single plasmon by two-level and V-type three-level quantum dot systems coupled to 1D waveguide, *Plasmonics* **10**, 1447 (2015).
- [64] T. S. Tsoi and C. K. Law, Single-photon scattering on Λ -type three-level atoms in a one-dimensional waveguide, *Phys. Rev. A* **80**, 033823 (2009).
- [65] W. Tian, B. Chen, and W.-D. Xu, Controlling single-photon transport along an optical waveguide by using a three-level atom, *Chin. Phys. Lett.* **29**, 030302 (2012).
- [66] R. Kokkonieni, T. Ollikainen, R. E. Lake, S. Saarenpää, K. Y. Tan, J. I. Kokkala, C. B. Dağ, J. Govenius, and M. Möttönen, Flux-tunable phase shifter for microwaves, *Sci. Rep.* **7**, 14713 (2017).